Biochemistry

 Volume 42, Number 29 July 29, 2003

Current Topics

Enzyme Electrokinetics: Using Protein Film Voltammetry To Investigate Redox Enzymes and Their Mechanisms†

Christophe Léger,‡ Sean J. Elliott,§ Kevin R. Hoke, Lars J. C. Jeuken,|| Anne K. Jones,⊥ and Fraser A. Armstrong*

Inorganic Chemistry Laboratory, Oxford University, South Parks Road, Oxford OX1 3QR, U.K.

Received May 14, 2003; Revised Manuscript Received June 2, 2003

ABSTRACT: Protein film voltammetry is a relatively new approach to studying redox enzymes, the concept being that a sample of a redox protein is configured as a film on an electrode and probed by a variety of electrochemical techniques. The enzyme molecules are bound at the electrode surface in such a way that there is fast electron transfer and complete retention of the chemistry of the active site that is observed in more conventional experiments. Modulations of the electrode potential or catalytic turnover result in the movement of electrons to, from, and within the enzyme; this is detected as a current that varies in characteristic ways with time and potential. Henceforth, the potential dimension is introduced into enzyme kinetics. The presence of additional intrinsic redox centers for providing fast intramolecular electron transfer between a buried active site and the protein surface is an important factor. Centers which carry out cooperative two-electron transfer, most obviously flavins, produce a particularly sharp signal that allows them to be observed, even as transient states, when spectroscopic methods are not useful. High catalytic activity produces a large amplification of the current, and useful information can be obtained even if the coverage on the electrode is low. Certain enzymes display optimum activity at a particular potential, and this can be both mechanistically informative and physiologically relevant. This paper outlines the principles of protein film voltammetry by discussing some recent results from this laboratory.

Important possibilities arise for extracting detailed information about the properties of redox enzymes that are attached to a suitable electrode surface (*1*, *2*). This is because the protein is "wired" directly to an instrument, i.e., the electrochemical analyzer, that simultaneously *activates* and *measures* redox chemistry; electron transfer is thus detected directly as electrical current, as functions of time and potential. Protein film voltammetry (PFV)[1] is a relatively new methodology, encompassing a suite of techniques,

† This work was supported by funds from BBSRC, EPSRC, Human Frontiers Science Program, EMBO, Rhodes Trust, and NSF.

* To whom correspondence should be addressed. Phone: 44-1865-272647. Fax: 44-1865-272690. E-mail: fraser.armstrong@chem.ox.ac.uk.

‡ Current address: Laboratoire de Bioénergétique et Ingénierie des Protéines, CNRS, 31 chemin Joseph Aiguier, 13402 Marseille, France.

§ Current address: Department of Chemistry, Boston University, 590 Commonwealth Ave., Boston, MA 02215.

|| Current address: Department of Physics and Astronomy, University of Leeds, Leeds LS2 9JT, U.K.

⊥ Current address: Institut für Biologie, Mikrobiologie, Humboldt-Universität zu Berlin, Chausseestr. 117, 10115 Berlin, Germany.

[1] Abbreviations: *A*, electrode area; *Av*-H_2ase, *A.* (formerly *Chromatium*) *vinosum* [NiFe]-hydrogenase; DMS, dimethyl sulfide; DMSO, dimethyl sulfoxide; DmsABC, *E. coli* DMSO reductase (holoenzyme); *E*, electrode potential, versus standard hydrogen electrode; ET, electron transfer; FAD, flavin adenine dinucleotide; FrdAB, *E. coli* fumarate reductase (soluble domain); Fcc$_3$, *S. frigidimarina* (NCIMB400) flavocytochrome c_3; *F*, Faraday constant; *i*, current; i_{lim}, limiting current at high driving force; MGD, molybdopterin guanine dinucleotide; NarGHI, *E. coli* nitrate reductase (holoenzyme); K_m, Michaelis−Menten constant; *n*, number of electrons transferred in an electrode process; Γ, coverage of the enzyme on the electrode (moles per square centimeter); ν, scan rate; ω, electrode rotation rate in units of revolutions per minute; PFV, protein film voltammetry; PGE, pyrolytic graphite edge; *R*, gas constant; SHE, standard hydrogen electrode; SWV, square-wave voltammetry; *T*, temperature.

10.1021/bi034789c CCC: $25.00
Published on Web 07/01/2003

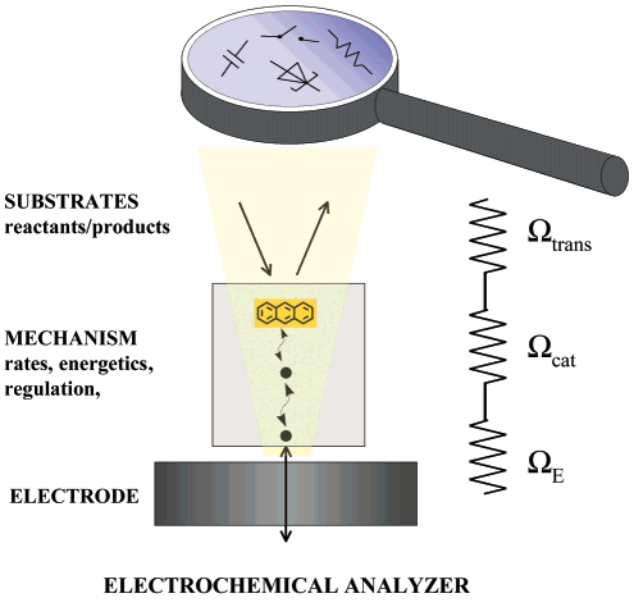

FIGURE 1: Cartoon showing a multicentered redox enzyme wired to an electrode in contact with a solution containing a substrate. The three stages of catalytic electron transport are represented as a series of resistors. In addition to the active site at which the substrate is transformed, the enzyme contains centers that are arranged in a relay to achieve long-range intramolecular electron transport. The magnifying glass represents our electrochemical view of the enzyme's components, including switches, resistors, capacitors (electron stores), and diodes.

and we introduce the concept with the cartoon shown in Figure 1.

A redox enzyme can be likened to a "mystery electronic device jettisoned by an alien spacecraft": we would wish to know what *it* does, so we would ask "what are its electronic characteristics?" To investigate, we would wire the device to an electronic probe to measure its current, voltage, and frequency responses. The relays, switches, gates, resistors, capacitors, diodes, and feedback circuits that are familiar in electronics have their representatives within the complex machinery of multicentered redox enzymes. Figure 1 shows how electron flow through the enzyme is linked in series to the rate of transport of the substrate to the electrode and to the rate of interfacial (electrode−enzyme) electron exchange. Conceptually, these stages resemble a series of resistors, each with a "conductance" equated with a transit time (in the language of enzyme kinetics). A key issue is then to arrange that the current−potential characteristics reflect the inherent properties of the enzyme, and not transport of substrate or interfacial (electrode−enzyme) electron transfer. Transport of the substrate can be driven hydrodynamically by rotating the electrode; this is itself a useful variable, since dispersal of the product can also be controlled to probe inhibition effects. More problematically, interfacial electron exchange depends on how buried the redox centers are and how effectively the enzyme makes electronic contact with the electrode surface; in this respect, current theories on distance and medium dependencies of electron coupling are important guides to the feasibility of achieving fast interfacial electron transfer in different cases (*3*, *4*). All being well, the investigator can hold an "interactive dialogue" with the enzyme.

Another view of PFV considers the electrode as a reaction partner that donates or accepts electrons over a continuous range of potential (driving force). Rates of redox processes and ensuing catalytic action respond in characteristic ways to variations in the electrode potential; therefore, PFV reveals the "potential dimension" in enzyme kinetics, providing a powerful method for investigating complex multicentered redox enzymes.

In general, the catalytic current reflects the properties of the electrochemical "control center", i.e., the redox site up to which there is fast and reversible electron exchange with the electrode. For most enzymes, intramolecular electron transfer is rapid so that the control center is the catalytic site, but cases may arise (such as conformational changes or domain movements) where the rate-determining step is an intramolecular electron transfer. The control center is then a relay site (such as a heme or Fe−S cluster) so that details of the catalytic action further up the line are not revealed. This concept is introduced in Figure 2, and we will refer to it later.

In this article, we describe studies that address the inherent properties of enzymes, and we will not emphasize applications such as biosensors or developments in electrode surfaces, good accounts of which are available (*5*, *6*). Even so, the interactions between proteins and electrode surfaces, interactions which are certainly dynamic and not static, are poorly understood (*7*−*9*). There is much interest in electrodes that can bind proteins and elicit fast interfacial electron transfer. These electrodes include carbon materials such as graphite, metal oxides, noble metals modified with various types of self-assembled monolayers, and electrodes coated with surfactants (*6*, *7*, *9*, *10*). Our discussions will focus on studies with graphite, in particular an electrode called pyrolytic graphite "edge" (PGE) produced by mounting pyrolytic graphite so that its basal (aromatic) layers are normal to the solution interface. Polishing with a gentle abrasive produces a rough surface that is rich in polar functionalities such as -COOH and -COH groups, and together with hydrophobic areas and solutes such as poly-ions (e.g., neomycin and polymyxin), these groups generate complex patches for protein adsorption (*8*). The large number of possible microenvironments renders the PGE electrode a "combinatorial" surface; i.e., there is a high probability that some enzyme molecules will bind productively. A protein film is formed by painting the electrode with a concentrated solution or by slow adsorption from a dilute solution; either way, the sample quantity actually being addressed is minuscule, on the picomole level. As discussed below, the electroactive coverage may not always be high enough to observe signals from stoichiometric oxidation or reduction of individual active sites, but much can still be learned when substrate is added, due to catalytic amplification of the current (*11*).

Nonturnover Voltammetry

In these experiments, we measure the current−potential response due to electron exchange between the electrode and the active sites of the enzyme, under conditions where there is no catalytic turnover (*1*, *2*). This situation is arranged (obviously) by having no substrate present, by blocking turnover with an inhibitor, or by modulating the potential at a sufficiently fast rate that a catalytic cycle cannot be

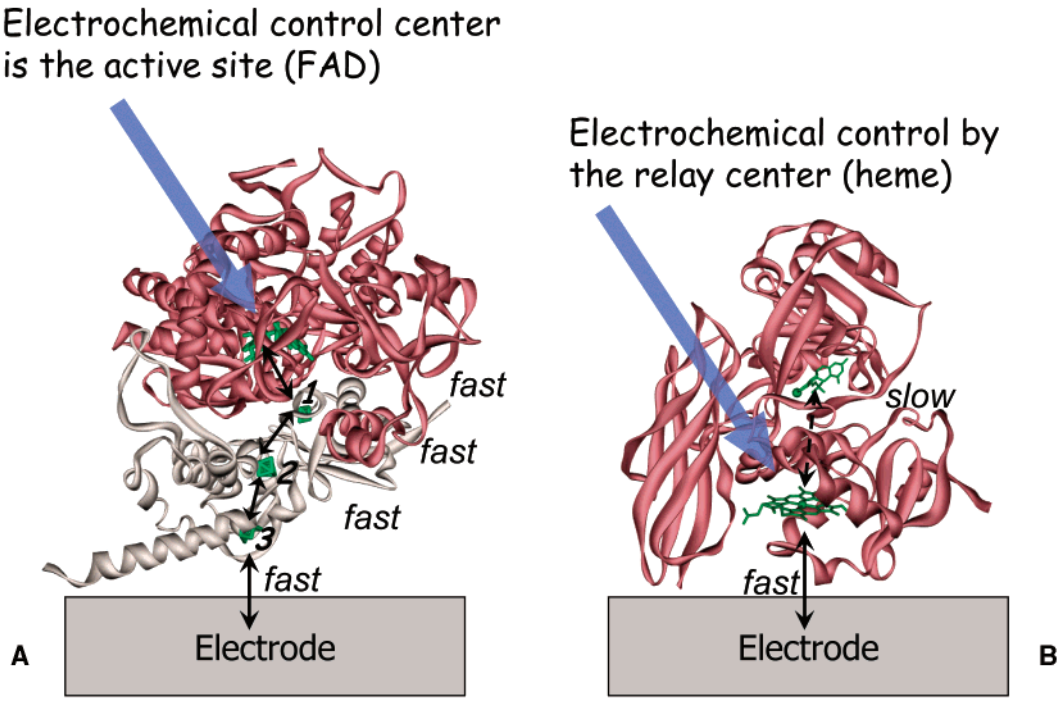

FIGURE 2: Concept of the electrochemical control center. (A) Fumarate reductase (FrdAB) from *E. coli* [adapted from the structure by Iverson et al. (*17*)]. Compared to the rate of turnover, electron transfer is relatively fast for all stages (interfacial and intramolecular) between the electrode and the FAD at the active site. All centers are detected in the nonturnover voltammogram. When the substrate is present (and its supply to the electrode is not a limiting factor), the catalytic response reflects the rate-determining transfer of electrons between the FAD and substrate. (B) Sulfite oxidase from chicken liver [monomer form, adapted from the structure of Kisker et al. (*43*)]. Interfacial electron exchange with the heme is fast, but intramolecular electron transfer is slow because only a small fraction of enzyme molecules on the electrode have the active site (Mo pterin) positioned at sufficiently close range (Mo and heme domains are separated by a linker peptide). The nonturnover experiment detects only the heme, while the catalytic response is small and reflects the properties of the heme rather than the Mo.

completed (examples of the latter are given later). Nonturnover experiments provide a "handle" analogous to a spectroscopic characteristic (like a chromophore) but with the added feature that the redox center is not only detected but also simultaneously *activated* (oxidized and reduced) under good electrochemical control. In a cyclic voltammetry experiment conducted at sufficiently low scan rates, the redox states of the active sites remain in ratios predicted by the Nernst equation, and the system is termed "reversible". In this case, the signal observed in a cyclic voltammetry experiment consists of a pair of current peaks—reduction and oxidation, each of finite area—produced as the electrode potential is swept across the formal reduction potential ($E^{\circ\prime}$) of the redox center in the negative (reducing) and positive (oxidizing) directions, respectively (*12*). The peak positions are similar in either direction (theoretically, they should be the same), and their average value approximates to $E^{\circ\prime}$ for the redox reaction.

To introduce the principles, Figure 3A shows a cyclic voltammogram for a small protein that (although not an enzyme) contains two redox centers that yield well-separated signals. The 7Fe ferredoxin from *Sulfolobus acidocaldarius* contains a [3Fe-4S] and a [4Fe-4S] cluster, and it adsorbs at a PGE electrode in the presence of polymyxin (*13*). Polymyxin contains several positively charged groups, and it acts as a noncovalent "cross-linker" between the negatively charged protein and acidic groups on the electrode surface (*9*). Sweeping the electrode potential in the negative direction produces successive reductions of the $[3Fe\text{-}4S]^{+/0/2-}$ and $[4Fe\text{-}4S]^{2+/+}$ clusters, and reversing the sweep results in their reoxidation. The peaks lie on a relatively large background due to electrode capacitance; this is removed to produce baseline-subtracted signals that are analyzed further.

For a one-electron redox process, each peak has an area proportional to $A\Gamma\nu$ (A is the electrode area, Γ the electroactive coverage, and ν the scan rate) so the voltammogram of a multicentered protein yields the number and stoichiometry of redox centers (*14*). In Figure 3A, the two signals at the highest and intermediate potentials have equal areas because they correspond to the $[3Fe\text{-}4S]^{+/0}$ and $[4Fe\text{-}4S]^{2+/+}$ couples, respectively, i.e., a 1:1 stoichiometry.

When more than one electron is transferred, the question arises of how the second transfer is influenced by the first. An important case is a *cooperative* two-electron reaction, one in which the second electron follows spontaneously after the first; i.e., $E^{\circ\prime}{}_2 > E^{\circ\prime}{}_1$ (*14*, *15*). This situation is encountered frequently with organic cofactors where the one-electron intermediate is inherently unstable, i.e., invariably for NAD^+ and commonly for flavins. A useful concept is the apparent n value, which represents the thermodynamic number of electrons that transfer in a single electrochemical event: the limiting n value of 2.0 for a fully cooperative two-electron reaction occurs when ΔE ($=E^{\circ\prime}{}_2 - E^{\circ\prime}{}_1$) > 180 mV, and it falls to 1.0 as ΔE decreases and the one-electron intermediate stabilizes (*15*). Since the half-height width of a peak is $91/n$ mV at 25 °C, and the peak current varies as n^2, a cooperative two-electron transfer gives a much sharper signal (*14*).[2] In Figure 3A, the larger signal observed at the more negative potential is due to the $[3Fe\text{-}4S]^{0/2-}$ transition,

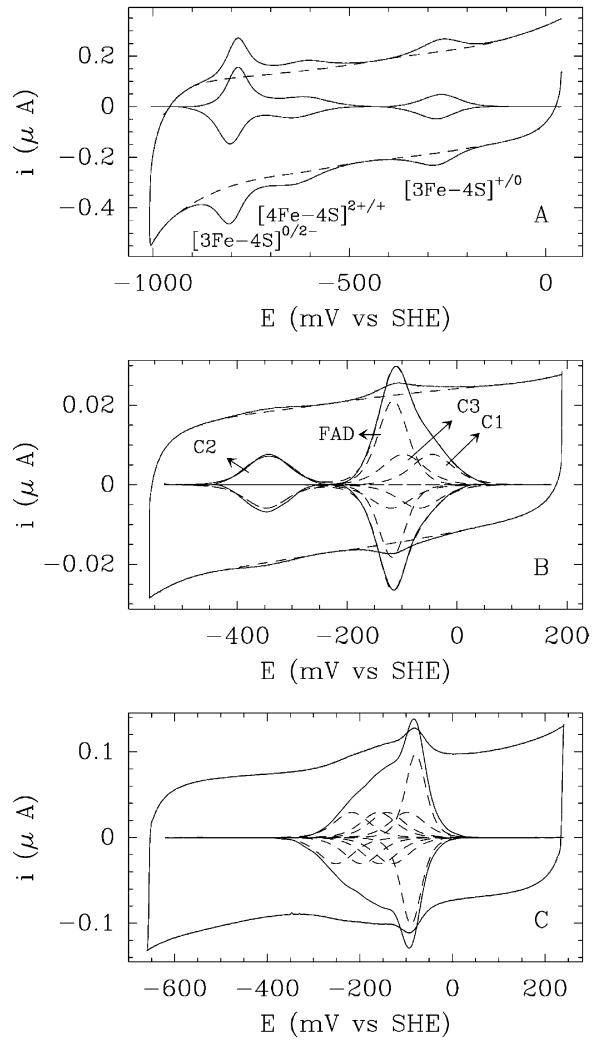

FIGURE 3: Examples of nonturnover cyclic voltammograms. The outer traces (not to scale) are raw voltammograms. The large background current (magnitude varies linearly with scan rate) is subtracted to give the faradaic signal of interest. The left-hand scale is for background-subtracted results. (A) *S. acidocaldarius* 7Fe ferredoxin, pH 8.0, $T = 15$ °C, $\nu = 50$ mV/s, and $\Gamma = 18$ pmol/cm^2. (B) Soluble subcomplex of *E. coli* fumarate reductase (FrdAB), pH 8.0, $T = 20$ °C, $\nu = 20$ mV/s, and $\Gamma = 6$ pmol/cm^2. (C) *S. frigidimarina* flavocytochrome c_3 (Fcc_3), pH 5.0, $T = 25$ °C, $\nu = 20$ mV/s, and $\Gamma = 21$ pmol/cm^2.

i.e., cooperative transfer of a further two electrons, an intriguing yet unresolved characteristic of [3Fe-4S] clusters (*13*).

These principles are used to study multicentered enzymes, in particular, those containing a flavin. Panels B and C of Figure 3 show how the redox centers of two much larger proteins, in this case, metalloflavoenzymes, are revealed in cyclic voltammograms. The membrane-bound fumarate reductase (Frd) from *Escherichia coli* is closely related to succinate dehydrogenase, most commonly encountered as mitochondrial Complex II (*16*, *17*). It contains a covalently bound FAD and three Fe−S clusters that are located in membrane-extrinsic subunits A and B, respectively. The FrdAB subcomplex is normally attached to the membrane by anchor peptides FrdC and FrdD that are required for interaction with quinones. FrdAB can be prepared by chemical or genetic modification: lacking its hydrophobic anchors, it is water soluble and adsorbs to high coverage on PGE, giving well-defined nonturnover signals (*15*, *18*, *19*). The structure of FrdAB and a schematic view of its electron transfers at the electrode are shown in Figure 2. The voltammogram (Figure 3B) shows a large asymmetric envelope of signals that can be deconvoluted to reveal components due to the FAD and Fe−S centers 1 ([2Fe-2S]) and 3 ([3Fe-4S]), and a signal at lower potential that is assigned to Fe−S center 2 ([4Fe-4S]). Center 2 lies between centers 1 and 3 and completes an electron relay between fumarate and menaquinol. The signals conform to the expected stoichiometry; importantly, the FAD is particularly prominent because it is a two-electron center with an inherently unstable semiquinone radical.

Figure 3C shows the voltammetry of another fumarate reductase, the soluble periplasmic flavocytochrome c_3 (Fcc_3) from *Shewanella frigidimarina*, which contains a noncovalently bound FAD and four *c*-type hemes (*20*). The fact that the voltammetry is dominated by the sharp contribution from the two-electron FAD is particularly significant in this case, since the UV−visible spectrum of the FAD is obscured by the intense bands from the four hemes. Voltammetry thus provides a unique handle on the flavin cofactor.

A similar situation has been identified recently for a Mo enzyme, arsenite oxidase from *Alcaligenes faecalis* (K. R. Hoke, N. Cobb, R. Hille, and F. A. Armstrong, unpublished results). Unusually, an EPR signal from Mo^V has not been observed for this enzyme, which also contains a [3Fe-4S] cluster and a Rieske [2Fe-2S] cluster; however, arsenite oxidase adsorbs on a PGE electrode (yielding catalytic electrochemistry when arsenite is present), and a prominent signal due to cooperative two-electron exchange is observed in the nonturnover experiments. This is the first example of a Mo enzyme operating in a highly cooperative two-electron Mo(VI/IV) manner, and voltammetry provides a handle for the active site that is complementary to the role normally played by EPR.

Many electrodes, such as PGE, can operate in aqueous solution over a wide potential range, so it is possible to observe redox transitions at very high potentials (generating powerful oxidants) or very low potentials (powerful reductants). The example of the [3Fe-4S]$^{0/2-}$ couple has been mentioned (Figure 3A), and this reaction is seen in many other proteins (*13*). Conversely, redox transitions due to the highly oxidizing intermediate of peroxidases (Compound I) are observed at potentials of >700 mV for cytochrome *c* peroxidase and its mutant forms, adsorbed on PGE (*21*). Reversible oxidation of the resting Fe(III) state of the enzyme is a cooperative two-electron process, and produces a prominent signal.

All the examples in Figure 3 arise from a high coverage of enzyme, typically 3−30 pmol/cm^2. More frequently, however, electroactive coverage may be insufficient to achieve detectable signals from electron exchange alone, and more sensitive techniques such as digital staircase voltammetry or square-wave voltammetry (SWV) are useful (*22*−*24*).

[2] In practical terms, peaks are usually broader and flatter than expected, due to heterogeneity among redox centers on the electrode (arising perhaps from variations in protein microenvironments). Consequently, a peak shape that conforms closely to theoretical expectations is an excellent indicator of the homogeneity of the system.

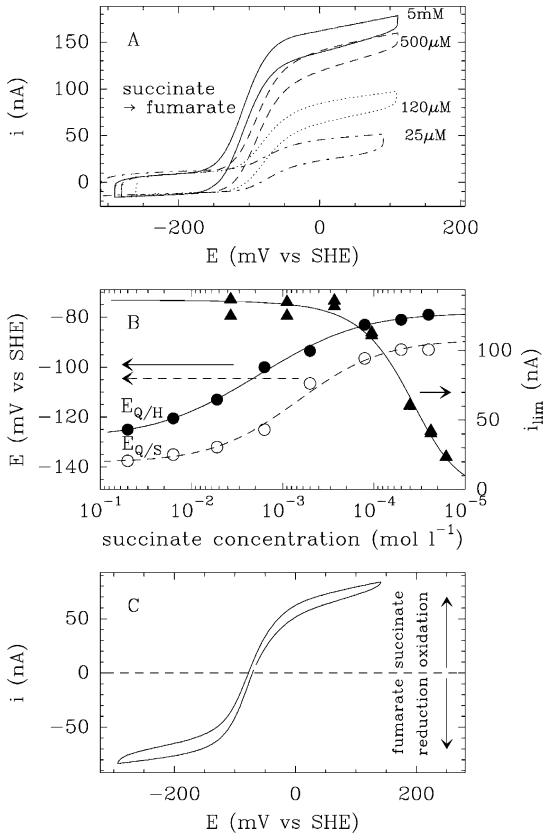

FIGURE 4: Different aspects of the catalytic voltammetry of *E. coli* fumarate reductase, FrdAB, at a PGE electrode. (A) Succinate oxidation by FrdAB (no fumarate present), pH 8.0, $T = 20$ °C, $\nu = 1$ mV/s, and $\omega = 3000$ rpm. (B) Circles and the left *Y*-axis show the dependence of the FAD two-electron and one-electron reduction potentials on succinate concentration (FAD species are quinone/hydroquinone, filled symbols and continuous line, and quinone/semiquinone, empty symbols and dashed line), with fit to eq 4 of ref *19*. Triangles and the right *Y*-axis show the dependence of i_{lim} on succinate concentration, and fit to the Michaelis−Menten equation (continuous line). (C) Catalytic bias; voltammogram measured in the presence of both substrates: 1.2 mM succinate, 4 μM fumarate, pH 7.0, $T = 20$ °C, $\nu = 1$ mV/s, and $\omega = 3000$ rpm.

Catalytic Voltammetry

Catalytic turnover produces a wave that generally has a sigmoidal shape. It is usually greatly magnified compared to the peak-like signals observed in the absence of substrate, and observable even if the enzyme is present only at low coverage.

Figure 4A shows catalytic voltammograms recorded for FrdAB adsorbed at a PGE electrode that is immersed in solutions containing various amounts of succinate (*19*). Oxidation of succinate is the reverse of the physiological reaction, and the slow turnover number ($k_{cat} < 15$ s^{-1} at pH 7) ensures that the current response reflects inherent properties of the enzyme rather than substrate transport or interfacial electron transfer (referring back to Figures 1 and 2). For each case, the catalytic wave (after removal of the capacitance background) is independent of the rate (this is sufficiently slow) and the direction of the potential scan; i.e., the system is at steady state. The catalytic wave shape is also independent of the electrode rotation rate, showing there are no substrate transport limitations (as expected, since the rate of turnover is low). This provides an important simplification, as described below.

The oxidation current represents the flux of electrons from succinate to the active site and then to the electrode, and it increases as the electrode potential is increased, reaching a limiting value i_{lim} at a potential corresponding to a sufficiently high driving force at which the active site effectively remains fully oxidized at steady state. As the succinate concentration is increased, i_{lim} increases in an analogous manner to the reaction velocity that would be measured in solution studies and analyzed in terms of Michaelis−Menten kinetics.[3] However, the wave also shifts to a more negative potential with an increasing succinate concentration. Closer examination shows further that the wave is not a simple sigmoid (it is steeper at low potential, at the onset of catalysis).[4] The current at all electrode potentials is proportional to the fraction of FAD in its fully oxidized (quinone) form, the active state for succinate oxidation. The Nernst equation links this fraction to the electrode potential and to the FAD reduction potentials that depend on pH and succinate concentration. The *n* value for FAD derived from the overall steepness of the wave is always less than 2.0 because the intermediate radical accumulates to small extents depending on succinate concentration. Modeling the wave shape yields both one-electron potentials of the FAD under ambient conditions while the enzyme is catalytically engaged. This contrasts with the reduction potentials determined by potentiometry, which reflect resting states of the enzyme.

In Figure 4B, these observations are modeled in terms of the contributions made at various succinate concentrations and electrode potentials by the three different oxidation states of the FAD; i.e., the components of the catalytic wave are identified with different intermediates that are formed during turnover. Plots of the active site reduction potentials as a function of succinate concentration or pH yield the substrate dissociation constants from all catalytic intermediates.[5] This information shows how electron transfers are coupled to substrate and proton binding during the catalytic cycle, and how the catalytic activity is revealed in the *potential dimension* (*19*). The FrdAB system exemplifies the concept of an *electrochemical control center*, identified here as the FAD. In Figure 2, electron transport between the FAD and the electrode is rapid and reversible, but beyond this (between succinate and FAD), it is slow.

An example in which the electrochemical control center is not the catalytic site but an electron relay center is provided by studies of sulfite oxidase from chicken liver (*25*). The catalytic site is a Mo coordinated to a pyranopterin-dithiolene,

[3] To proceed with confidence to interpret PFV data, it is important that the electrochemical activity is comparable to (or higher than) the activity measured by conventional kinetic methods. To determine the turnover number (k_{cat}), it is necessary to know the electroactive coverage that is measured under noncatalytic conditions (see the previous section and Figure 3), although, sometimes, the coverage may be insufficient for detection of enzyme molecules without the amplification from catalysis. On the other hand, the Michaelis constant can always be determined from the *relative* change in i_{lim} against substrate concentration (▲ and right *Y*-axis in Figure 4B), provided the (possibly unknown) coverage is constant.

[4] The detailed form of the wave is visualized more clearly in a plot of $\log[i_{lim}/(i - 1)]$ against potential (a Heyrovsky−Ilkovitch plot). This is described further in ref *19*.

[5] The shift of the catalytic wave to a more negative potential as succinate is added (Figure 4B) arises because succinate binds more tightly when the FAD is fully oxidized or half-oxidized (see the later discussion and Figure 8B).

while electrons are relayed to the natural partner by a single heme located on a separate, mobile domain. The enzyme is actually a homodimer, each monomer consisting of Mo, heme, and linker domains. Nonturnover experiments give only a signal from the heme, while addition of the substrate gives a catalytic wave that reflects the properties of the heme rather than the Mo (activity is low, the *n* value is 1.0, and the position is not sensitive to pH or sulfite concentration as would be expected if the Mo cofactor were the control center). Evidently, on the electrode, the rate-determining step is intramolecular ET, as represented in Figure 2.[6] Another example is a complex between cytochrome *c* oxidase and cytochrome *c* adsorbed on an Au electrode modified with 3-mercapto-1-propanol (*10*). The voltammetry shows a nonturnover signal due to cytochrome *c*, but the catalytic wave that is obtained in the presence of O_2 has an amplitude that is much lower than expected, and occurs at a potential corresponding to that of the mediating cytochrome. Fast electron transfer is thus effective only as far as cytochrome *c* (the electrochemical control center in this case), and there is some problem with the protein−protein orientation that prevents fast transfer from cytochrome *c* into the enzyme.

One of the simplest demonstrations with PFV is that of catalytic bias, i.e., the degree to which a redox enzyme is biased to operate in one particular direction. Figure 4C shows that for FrdAB, at pH 7, the succinate oxidation current produced by 1.2 mM succinate is equal to the reduction current given by just 4 μM fumarate (*19*).[7] Fumarate reduction (the assumed physiological reaction) is actually so fast that the current response is complicated by mass transport. (For Figure 4C, the electrode was rotated at a high frequency; otherwise, the fumarate reduction component is attenuated.) A similar experiment has demonstrated that succinate dehydrogenase is actually a very good fumarate reductase (*26*, *27*).

The ability of PFV to address each of the different stages depicted in Figure 1 is demonstrated in studies of *Allochromatiun vinosum* [NiFe]-hydrogenase (*Av*-H_2ase) (*28*−*31*). The active site, an unusual binuclear Ni−Fe center, is buried well within the enzyme, and electrons are relayed to the natural reaction partner (or electrode) by three Fe−S clusters.

Adsorbed on a PGE electrode, *Av*-H_2ase exhibits remarkably high activity, as illustrated in Figure 5A, which shows catalytic voltammograms recorded for 0.1 bar H_2 at 30 °C (*28*). The oxidation current increases with electrode rotation rate because the H_2 oxidation activity is so high that the current is limited by transport of H_2 to the electrode. A useful diagnostic tool is the so-called Levich relationship, a plot of current against the square root of the rotation rate, which is linear if the current is controlled by mass transport (*12*). In this case it is. More frequently, the current levels off at high rotation rates, and a plot of the inverse current versus the inverse square root of the rotation rate (a Koutecky−Levich plot) allows extrapolation to an infinite rotation rate, at which

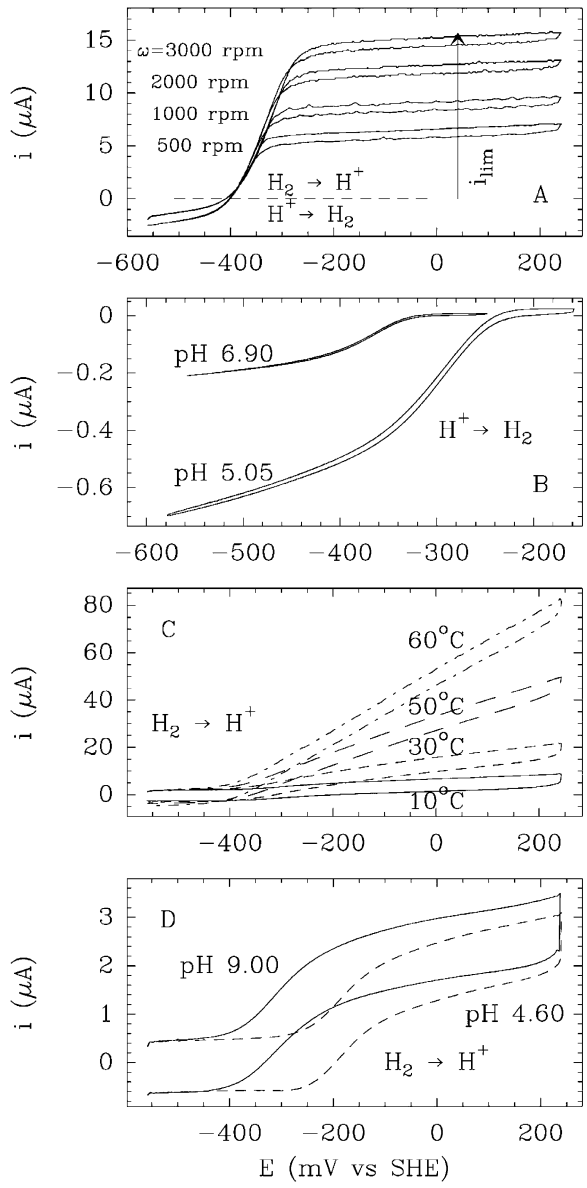

FIGURE 5: Different aspects of the catalytic voltammetry of *A. vinosum* [NiFe]-hydrogenase (*Av*-H_2ase) adsorbed at a PGE electrode, recorded under the conditions given below. (A) Mass transport-controlled H_2 oxidation: 0.1 bar H_2, pH 6.5, $T = 30$ °C, and $\nu = 100$ mV/s. (B) Proton reduction: 1 bar N_2, $T = 5$ °C, $\omega = 6000$ rpm, $\nu = 3$ mV/s (pH 6.9) and 6 mV/s (pH 5.1). (C) Electron transfer-controlled H_2 oxidation: 1 bar H_2, pH 7, $\omega = 2500$ rpm, and $\nu = 1$ V/s. (D) Enzyme-controlled H_2 oxidation: 1 bar H_2, $T = 5$ °C, $\omega = 2000$ rpm, and $\nu = 200$ mV/s.

the catalytic rate is controlled by the inherent properties of the enzyme (*18*).

In the case of *Av*-H_2ase, coverage is low, and it is difficult to quantify the number of active enzyme molecules on the electrode surface; however, close inspection of voltammograms measured in the absence of H_2 often reveals a small signal at approximately −30 mV, in the region expected for the [3Fe-4S] cluster, consistent with a maximum coverage of 3 pmol/cm^2. On the basis of this upper limit, the turnover number for H_2 oxidation at 30 °C exceeds 1500 s^{-1}, a value that is substantially higher than that measured using soluble dyes as electron acceptors (*28*). This suggests that in conventional solution assays, the rate is limited by the reaction with the soluble electron acceptor and not by H_2

[6] A recent study has been reported for a bacterial sulfite oxidase in which the Mo and heme domains are not separated by a linker. Both redox centers can be observed in nonturnover voltammograms, although the stoichiometries are not clear, and the catalytic rates are in accordance with those expected from conventional kinetics (*42*).

[7] The exact magnitude of this catalytic bias must be determined by more detailed studies that include consideration of the binding constants for fumarate and succinate to each redox state of the enzyme (*19*).

oxidation at the active site. The PGE electrode appears to be a superior artificial redox partner because electrons (or holes) are effectively "on tap".

The negative current at low potentials in Figure 5A results from the catalytic reduction of H^+ to evolve H_2, and Figure 5B shows how this is investigated further under an N_2 atmosphere (*30*). Significantly, there is still a dependence on electrode rotation rate, even at low temperatures (the experiment whose results are shown was carried out at 6000 rpm and 5 °C). In contrast with experiments whose results are depicted in panel A, this dependence is not due to supply and depletion of substrate (in this case H^+) but to dispersion of the product, H_2, which strongly inhibits H^+ reduction if it accumulates in the vicinity of enzyme molecules on the electrode surface. Electrode rotation is thus exploited to observe and control product inhibition.

The potential range, shape, and amplitude of the catalytic wave for H^+ reduction are dependent on pH, and detailed analysis sheds important light on the mechanism (*30*). The voltammograms in Figure 5B show that the current at low potentials does not level off at a limiting value, as expected, but displays a residual slope. This observation is mechanistically significant, and is particularly noticeable in the direction of H_2 oxidation, for which a dramatic alteration in the wave shape is observed as the temperature is increased (Figure 5C). In these experiments, control by H_2 transport (the rotation rate dependence) was removed by lightly polishing the electrode to decrease the enzyme coverage and by increasing the H_2 partial pressure to 1 bar (*31*). The nearly sigmoidal wave observed at low temperatures (see panel D for an enlarged scale, similar conditions) converts to a response that is *linear* over a potential range of more than 0.5 V when the temperature is increased to 60 °C (*31*). This behavior arises from heterogeneity in the adsorbed protein layer, and the contribution of enzyme molecules having poorer electron coupling with the electrode (lower interfacial ET rate constants), which contribute to turnover only at a greater driving force. The slope reflects the competition between the enzyme's catalytic activity and the rates of interfacial electron transfer. The increase in linearity as the temperature is increased can be understood in terms of there being a lower activation energy for interfacial electron transfer than for catalytic turnover.[8]

Figure 5D shows voltammograms for a low-coverage film of hydrogenase catalyzing H_2 oxidation (1 bar) at two different pH values. The experiment demonstrates that while the position of the catalytic wave shifts considerably with pH, the approximate limiting current does not. The contrast with H^+ reduction (Figure 5B) can be understood in terms of the rate-determining step in H_2 oxidation involving only *one* protonation state of the enzyme, while H_2 evolution stems from *two* different protonation states, hence the contrast in current magnitudes (*30*). Importantly, unlike a chemical electron donor or acceptor, the electrode can take the potential to whatever value is required to attain the true inherent catalytic limiting rate under any conditions. Inspection of Figure 5D shows how, using a chemical electron donor with which equilibrium is established rapidly at approximately −250 mV, the rate of H_2 oxidation would appear to be high at pH 9.0 but negligible at pH 4.6.

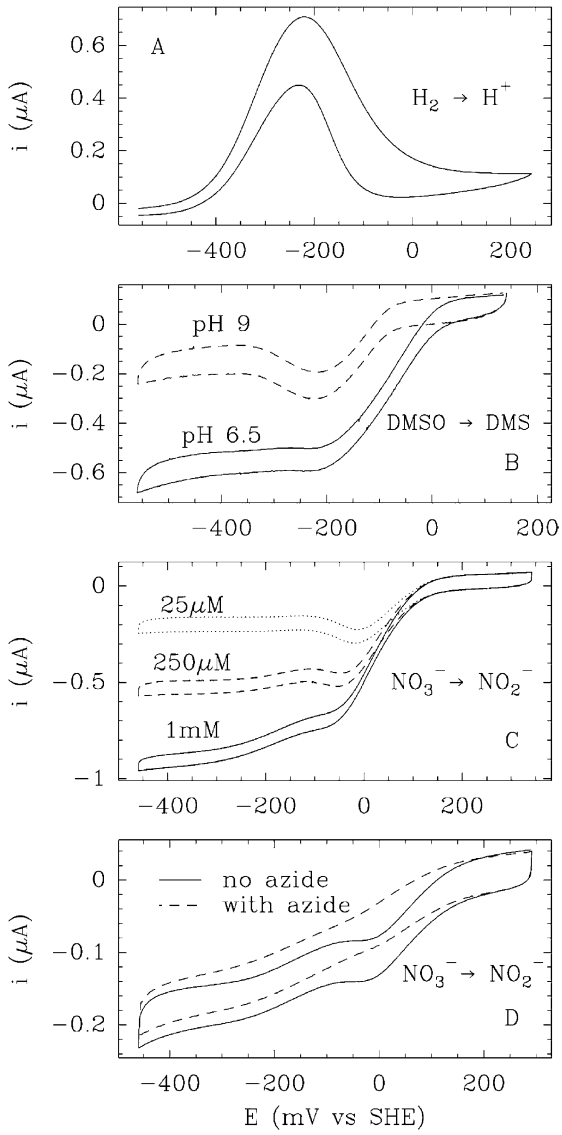

FIGURE 6: Activity switches (potential optima) exhibited by *Av*-H_2ase and two Mo enzymes. (A) Oxidation of H_2 by *Av*-H_2ase. When a very low scan rate is used, the enzyme is observed to switch reversibly to an inactive form at a high potential: 1 bar H_2, pH 9.0, T = 45 °C, ω = 1500 rpm, and ν = 0.3 mV/s. (B) Potential optimum exhibited by *E. coli* DMSO reductase (DmsABC) for the reduction of DMSO: 20 mM DMSO, pH 6.5 (continuous line) and 9.0 (dashed line), T = 25 °C, ω = 0 rpm (stationary electrode), and ν = 5 mV/s. (C) Potential optima exhibited by *E. coli* nitrate reductase (NarGHI) for the reduction of different concentrations of nitrate: pH 7.0, T = 30 °C, ω = 2000 rpm, and ν = 10 mV/s. (D) Effect of adding azide (N_3^-) on the catalytic response for nitrate reduction by NarGHI: pH 7.0, 25 °C, ω = 2000 rpm, and ν = 10 mV/s. Concentrations are 0.1 mM nitrate without azide and 1 mM nitrate with 1 μM azide.

Figure 6 shows different examples in which catalytic activity of an enzyme *decreases* in opposition to the electrode potential becoming more favorable. First, we return to *Av*-H_2ase, for which the voltammogram in Figure 6A has been measured at a very slow scan rate. This reveals the interconversion between the active enzyme and an oxidized

[8] Interestingly, the linear relationship that exists between the slope and turnover rate implies that measurement of the limiting current at a high driving force can be substituted by measurement of the slope. This is useful in cases where the activity does not level off in the experimental range of electrode potentials; for example, the change in slope as a function of temperature has been used to measure the activation energy of catalytic H_2 oxidation (*31*).

inactive Ni(III) state in which an additional ligand, believed to be OH^-, has become coordinated (*32*). The H_2 oxidation activity drops as the potential is increased, but is recovered on the reverse scan, as the active site switches rapidly back to the Ni(II) state and releases the inhibitory ligand; consequently, H_2 oxidation exhibits a *potential optimum.* The potential dependence and kinetics of the transformations can be deconvoluted with another technique, chronoamperomery, in which a potential step is used to activate the reaction and the time course of the resulting current is measured (*32*).

Potential optima for catalytic activity may indeed be a common property of redox enzymes, analogous to familiar pH optima (*33*). Examples are to be found with Mo enzymes in which the active site can exist in states Mo(IV), Mo(V), and Mo(VI), not to mention the different oxidation states possible for the pterin cofactor(s). Figure 6B shows that DMSO reductase from *E. coli* efficiently catalyzes the reduction of DMSO to DMS, but at pH 9, this activity is optimized in a narrow potential window that correlates with the maximum stability of the active site Mo(V) state (the active site is a Mo-bisMGD center, where MGD is molybdopterin guanine dinucleotide) (*34*). This result was interpreted in terms of the rate-determining step being facilitated when the active site is in the intermediate Mo(V) oxidation state. Figure 6C shows the profile for reduction of nitrate by *E. coli* nitrate reductase, which also contains Mo-bisMGD as the active site (*35*). At very low nitrate concentrations, the activity reaches a maximum and then drops to negligible levels as the potential is reduced further. As more nitrate is added, catalytic activity builds up at more negative potentials, and this eventually takes over as the dominant characteristic at high nitrate concentrations. One interpretation is that although Mo(IV) is an essential intermediate in the catalytic cycle, nitrate actually binds more tightly to Mo(V); in other words, K_m is much lower. Thus, contrary to simple expectations, low levels of nitrate are reduced only at high potentials.

This concept can be pursued further by adding an inhibitor that competes with substrate binding but has a strong preference for a particular redox state of the active site. Figure 6D shows that the local activity optimum around −50 mV disappears when azide (N_3^-) is added. This is a known inhibitor, but it is also a "hard" ligand that is expected to bind more tightly to Mo(V) than to Mo(IV).

Potential optima effects have been observed with *Paracoccus pantotrophus* nitrate reductase (soluble domain), and correlations have been made with EPR spectroscopic titrations of the Mo center (*36*). A potential optimum is also seen in experiments carried out on the multi-heme enzyme nitrite reductase, in which the activity for six-electron reduction of nitrite to ammonia drops below a certain potential (*37*). Notably, this effect was first detected for succinate dehydrogenase from mitochondria (later also from *E. coli*) for which the rate of fumarate reduction *decreases* when the electrode potential becomes too negative (*26, 27, 38*). It was remarked that the decrease in activity as the driving force is increased resembles the action of a tunnel diode, an electronic device displaying negative resistance (*38*). This property may have a physiological function, such as the rapid regulation of activity of respiratory chains (*33*).

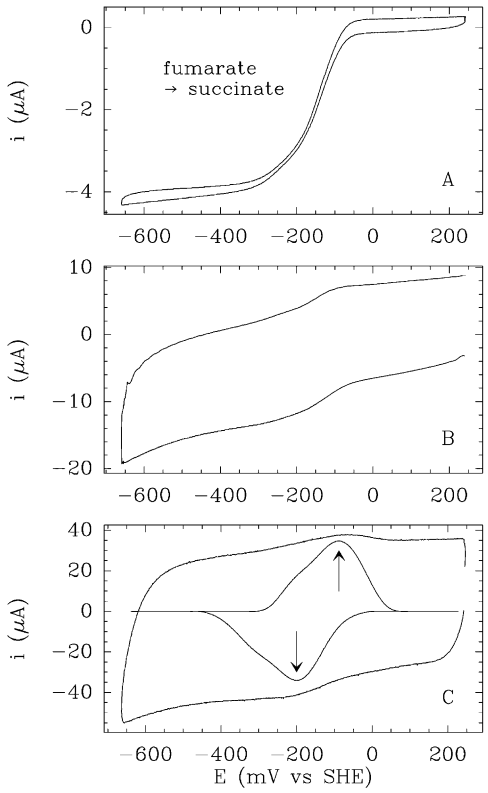

FIGURE 7: Voltammetry of a film of Fcc_3 in the presence of fumarate showing the effect of increasing the potential scan rate to a value that outruns the catalytic cycle (*39*). The solution contained 0.42 mM fumarate at pH 7.0, $T = 10$ °C, $\omega = 1500$ rpm, and $\nu =$ 10 mV/s (A), 1 V/s (B), and 82 V/s (C). Panel C also shows baseline-subtracted data, with the prominent component from the FAD highlighted with arrows.

Fast Voltammetry and Detection of Transient States

In these experiments, the electrons are moved rapidly within the enzyme by employing a fast potential modulation. This can provide insight into the rates and mechanisms of intramolecular electron transfer and allow detection of transient catalytic intermediates.

Figure 7 shows cyclic voltammograms for a film of Fcc_3 on a PGE electrode in a solution containing 0.42 mM fumarate ($>10K_m$), and recorded at scan rates of 10 mV/s, 1 V/s, and 80 V/s (*39*). As the scan rate is increased, the sigmoidal waveform converts to a composite peak-like signal (Figure 7C) resembling that obtained in the absence of substrate.[9] The reappearance of the sharp component due to the FAD (although this is broadened compared with the result obtained at low scan rate, shown in Figure 3C) shows that on this faster time scale both the required electrons are transferred through the enzyme to the FAD, and then both are "re-called" to the electrode before they can be passed to the substrate. The catalytic cycle is therefore outrun, and the flavin is detected as a transient, in this case on the millisecond time scale. The fact that this transient voltammetric signal contains no additional features or increased faradaic capacity shows that the bound substrate molecule does not provide an additional electroactive component on this time scale; therefore, product dissociation is not rate-determining. It

[9] The peak separation reflects the fact that ET is not infinitely fast with respect to the time scale of the experiment.

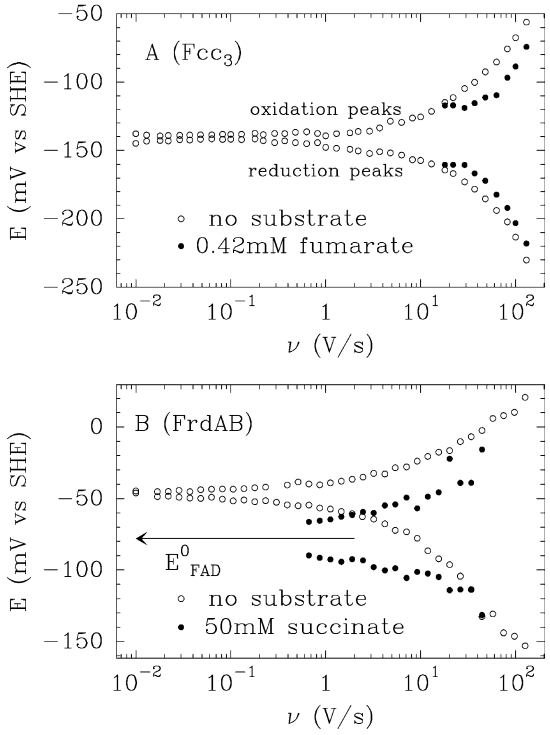

FIGURE 8: Trumpet plots showing how peak positions due to the FAD group of fumarate reductases vary with scan rate (ν in volts per second) and the introduction of substrates. (A) *S. frigidimarina* Fcc_3 without substrate (○) and in the presence of 0.42 mM fumarate (●) at pH 7.0 and 10 °C. (B) *E. coli* FrdAB without substrate (○) and in the presence of 50 mM succinate (●) at pH 7 and 20 °C. In panel B, the arrow marks the value of the reduction potential of the FAD in FrdAB in the presence of 50 mM succinate.

would otherwise be possible to move four electrons rather than two, back and forth between the electrode and the FAD.

From the appearance and positions of oxidation and reduction peaks as a function of scan rate, it is possible to determine not only the standard rate constant for electron exchange (k_0 is obtained by fitting the data) but also how electron transfer is coupled to chemical processes (*40*, *41*).[10] The data are displayed as a "trumpet plot", which monitors the active site in different time domains (*1*, *2*). Two such plots are shown in Figure 8.

Figure 8A shows results obtained with Fcc_3, in which the peak positions for the FAD signal are measured in the absence and presence of fumarate (*39*). Without substrate, the data are continuous throughout the range of scan rates. The left side (low scan rates) provides data about the slow time scale, analogous to those obtained in a potentiometric experiment; i.e., there is plenty of time for the system to equilibrate. The right side (fast scan rates) shows how the FAD behaves on the millisecond time scale: under these conditions (pH 7), the reduction potential (the average of the oxidation and reduction peak potentials) is very similar to that observed for the slow time scale; therefore, the processes necessary for establishing equilibrium (arrival and departure of two electrons as well as the necessary number of protons, and relaxation around the active site) have *all* occurred within the fast cycle. When fumarate is present, the nonturnover signal is replaced with a catalytic wave, and the FAD peaks are not observed until the scan rate is sufficiently high (Figure 7) to outrun catalysis. When they do appear, at ~20 V/s, it is clear that the reduction potential (obtained from the average of the oxidation and reduction peak potentials) is similar to that observed when no fumarate is present. Therefore, fumarate binds with the same affinity regardless of whether the FAD is oxidized or reduced. Notably, the decreased peak separation shows that the rate of electron transfer to the FAD is higher for the enzyme−substrate complex. Similar observations have been made for *E. coli* FrdAB in the presence of fumarate.

A different result is obtained with succinate, as shown in Figure 8B, in this case for FrdAB (Fcc_3 is inactive for succinate oxidation) (*19*). Because the turnover rate in this direction is much lower, the FAD peaks make their appearance below 1 V/s, and the observation that the FAD reduction potential is more negative when succinate is bound is consistent with the shift observed in the catalytic wave (Figure 4A) discussed earlier.

Square-wave voltammetry (SWV) provides an alternative way of driving electron transfers in an adsorbed enzyme. Whereas with cyclic voltammetry the potential is varied in a linear or shallow staircase manner, SWV uses a square-shaped potential modulation superimposed upon a shallow staircase background. By varying the frequency and amplitude of this modulation, one can obtain information about rates and energetics of electron transfer (*23*, *24*). Large potential modulations can be used to measure how sensitive a process is to the electrochemical driving force. For example, does varying the electrochemical driving force have a significant effect on the rate of redox cycling of an active site located at the end of a chain of relay centers? This is relevant to the question of whether electron transport occurs by hopping or superexchange (*23*). According to Marcus theory, the rate of a simple electron transfer reaction at an electrode reaches a limiting value (k_{max}) when the driving force is much greater than the reorganization energy (*11*). Electrochemists normally use a controlled potential step technique called chronoamperometry to measure electrode kinetics as a function of potential, but this is unsuitable for studies of a monolayer of protein molecules (*12*). First, the current due to electron transfers is small and usually masked by the large current due to electrode double-layer charging (this is particularly problematic with PGE); second, most enzymes contain several redox centers, and it is important to isolate the one of interest. SWV overcomes these problems as it allows the use of large potential steps to vary the driving force, while probing also the potential dimension to distinguish rates for different centers.

Given the complexity of this approach and the constraints of space, we refer to recent papers that describe results obtained by SWV (*23*, *24*). In several cases, it is found that k_{max} values are much lower than expected from Marcus theory, and suggest that electron transfer is attenuated by other processes, such as fluctuations in protein orientation. While the data for FrdAB could be fitted to a model in which electron transfer between the FAD and PGE occurs by hopping along the relay of Fe−S clusters, the results obtained

[10] For example, the buried [3Fe-4S] cluster in *Azotobacter vinelandii* ferredoxin I takes up a proton when it is reduced from the "+" to the "0" level. By recording the peak positions for the $[3Fe\text{-}4S]^{+/0}$ signal over a wide range of scan rates, from 10 mV s^{-1} to 100 V s^{-1}, and extending this to several structurally defined mutated forms, we determined the mechanism of proton transfer to and from the cluster (a mobile carboxylate side chain is used as a courier) (*40*).

for Fcc_3 could only be fit on the basis of a *direct* process, raising the likelihood that ET occurs via a superexchange mechanism utilizing the heme groups to enhance electronic coupling.

Concluding Remarks

Protein film voltammetry is a relatively new concept which explores largely uncharted territory, and it offers many interesting opportunities for fundamental and applied research. This article has aimed to outline the ideas and identify the special information that can be acquired. Among the chemical challenges are the problems of synthesizing and characterizing electrode surfaces that are better defined structurally and more realistic biologically, as well as producing fast interfacial ET. Another direction is the application of specialized spectroscopic methods to complement and exploit (e.g., using potential modulation) the excellent electrochemical activities of many adsorbed proteins. For the enzymologists, there are opportunities to understand complex, membrane-bound systems in ways analogous to characterizing an electronic component by its current−voltage response. This may be particularly true in bioenergetics, where some aspects of metabolic control may be determined at the membrane/electrochemical level.

ACKNOWLEDGMENT

We thank Brian A. C. Ackrell, Siem P. J. Albracht, Francis Blasco, Gary Cecchini, Steve Chapman, John Enemark, Nicolas Ginet, Russ Hille, Richard A. Rothery, and Joel H. Weiner for invaluable, ongoing collaborations and Libei Bateman, Kerensa Heffron, Janette Hudson, Sophie Lamle, James McEvoy, Harsh R. Pershad, and Emma Sillery for their contributions to some of the recently discussed ideas and experiments.

REFERENCES

1. Armstrong, F. A., Heering, H. A., and Hirst, J. (1997) *Chem. Soc. Rev. 26*, 169−179.
2. Armstrong, F. A. (2002) *J. Chem. Soc., Dalton Trans.*, 661−671.
3. Bendall, D. S., Ed. (1996) *Protein Electron Transfer*, Bios Scientific Publishers, Oxford, U.K.
4. Page, C. C., Moser, C. C., Chen, X. X., and Dutton, P. L. (1999) *Nature 402*, 47−52.
5. Kano, K., and Ikeda, T. (2003) *Electrochemistry 71*, 86−99.
6. Rusling, J. F. (1998) *Acc. Chem. Res. 31*, 363−369.
7. Baymann, F., Barlow, N. L., Aubert, C., Schoepp-Cothenet, B., Leroy, G., and Armstrong, F. A. (2003) *FEBS Lett. 539*, 91−94.
8. Armstrong, F. A., Camba, R., Heering, H. A., Hirst, J., Jeuken, L. J. C., Jones, A. K., Léger, C., and McEvoy, J. P. (2000) *Faraday Discuss. 116*, 191−203.
9. Armstrong, F. A., and Wilson, G. S. (2000) *Electrochim. Acta 45*, 2623−2645.
10. Haas, A. S., Pilloud, D. L., Reddy, K. S., Babcock, G. T., Moser, C. C., Blasie, J. K., and Dutton, P. L. (2001) *J. Phys. Chem. B 105*, 11351−11362.
11. Heering, H. A., Hirst, J., and Armstrong, F. A. (1998) *J. Phys. Chem. B 102*, 6889−6902.
12. Bard, A. J., and Faulkner, L. R. (2001) *Electrochemical methods. Fundamental and applications*, John Wiley & Sons, New York.
13. Duff, J. L. C., Breton, J. L., Butt, J. N., Armstrong, F. A., and Thomson, A. J. (1996) *J. Am. Chem. Soc. 118*, 8593−8603.
14. Plichon, V., and Laviron, E. (1976) *J. Electroanal. Chem. 71*, 143−156.
15. Heering, H. A., Weiner, J. H., and Armstrong, F. A. (1997) *J. Am. Chem. Soc. 119*, 11628−11638.
16. Ohnishi, T., Moser, C. C., Page, C. C., Dutton, P. L., and Yano, T. (2000) *Structure 8*, R23−R32.
17. Iverson, T. M., Luna-Chavez, C., Cecchini, G., and Rees, D. C. (1999) *Science 284*, 1961−1966.
18. Sucheta, A., Cammack, R., Weiner, J. H., and Armstrong, F. A. (1993) *Biochemistry 32*, 5455−5465.
19. Léger, C., Heffron, K., Pershad, H. R., Maklashina, E., Luna-Chavez, C., Cecchini, G., Ackrell, B. A. C., and Armstrong, F. A. (2001) *Biochemistry 40*, 11234−11245.
20. Turner, K. L., Doherty, M. K., Heering, H. A., Armstrong, F. A., Reid, G. A., and Chapman, S. K. (1999) *Biochemistry 38*, 3302−3309.
21. Mondal, M. S., Goodin, D. B., and Armstrong, F. A. (1998) *J. Am. Chem. Soc. 120*, 6270−6276.
22. Heering, H. A., Mondal, M. S., and Armstrong, F. A. (1999) *Anal. Chem. 71*, 174−182.
23. Jeuken, L. J. C., Jones, A. K., Chapman, S. K., Cecchini, G., and Armstrong, F. A. (2002) *J. Am. Chem. Soc. 124*, 5702−5713.
24. Jeuken, L. J. C., McEvoy, J. P., and Armstrong, F. A. (2002) *J. Phys. Chem. B 106*, 2304−2313.
25. Elliott, S. J., McElhaney, A. E., Feng, C., Enemark, J. H., and Armstrong, F. A. (2002) *J. Am. Chem. Soc. 124*, 11612−11613.
26. Hirst, J., Achrell, B. A. C., Sucheta, A., and Armstrong, F. A. (1996) *J. Am. Chem. Soc. 118*, 7434−7439.
27. Hirst, J., Ackrell, B. A. C., and Armstrong, F. A. (1997) *J. Am. Chem. Soc. 119*, 7434−7439.
28. Pershad, H. R., Duff, J. L. C., Heering, H. A., Duin, E. C., Albracht, S. P. J., and Armstrong, F. A. (1999) *Biochemistry 38*, 8992−8999.
29. Jones, A. K., Sillery, E., Albracht, S. P. J., and Armstrong, F. A. (2002) *Chem. Commun.*, 866−867.
30. Léger, C., Jones, A. K., Roseboom, W., Albracht, S. P. J., and Armstrong, F. A. (2002) *Biochemistry 41*, 15736−15746.
31. Léger, C., Jones, A. K., Albracht, S. P. J., and Armstrong, F. A. (2002) *J. Phys. Chem. B 106*, 13058−13063.
32. Jones, A. K., Lamle, S. E., Pershad, H. R., Vincent, K. A., Albracht, S. P. J., and Armstrong, F. A. (2003) *J. Am. Chem. Soc.* (in press).
33. Elliott, S. J., Léger, C., Pershad, H. R., Hirst, J., Heffron, K., Ginet, N., Blasco, F., Rothery, R. A., Weiner, J. H., and Armstrong, F. A. (2002) *Biochim. Biophys. Acta 1555*, 54−59.
34. Heffron, K., Léger, C., Rothery, R. A., Weiner, J. H., and Armstrong, F. A. (2001) *Biochemistry 40*, 3117−3126.
35. Elliott, S. J., Hoke, K. R., Rothery, R. A., Weiner, J. H., and Armstrong, F. A. (2003) (manuscript in preparation).
36. Anderson, L. J., Richardson, D. J., and Butt, J. N. (2001) *Biochemistry 40*, 11294−11307.
37. Angove, H. C., Cole, J. A., Richardson, D. J., and Butt, J. N. (2002) *J. Biol. Chem. 277*, 23374−23381.
38. Sucheta, A., Ackrell, B. A. C., Cochran, B., and Armstrong, F. A. (1992) *Nature 356*, 361−362.
39. Jones, A. K., Camba, R., Reid, G. A., Chapman, S. K., and Armstrong, F. A. (2000) *J. Am. Chem. Soc. 122*, 6494−6495.
40. Chen, K., Hirst, J., Camba, R., Bonagura, C. A., Stout, C. D., Burgess, B. K., and Armstrong, F. A. (2000) *Nature 405*, 814−817.
41. Hirst, J., and Armstrong, F. A. (1998) *Anal. Chem. 70*, 5062−5071.
42. Aguey-Zinsou, K.-F., Bernhardt, P. V., Kappler, U., and McEwan, A. G. (2003) *J. Am. Chem. Soc. 125*, 530−535.
43. Kisker, C., Schindelin, H., Pacheco, A., Wehbi, W. A., Garrett, R. M., Rajagopalan, K. V., Enemark, J. H., and Rees, D. C. (1997) *Cell 91*, 973−983.

BI034789C